1 <div align="center">Supporting Information</div>

2 **Dual-outward contraction induced construction of 2D hollow carbon**

3 **superstructures**

4 Yaqi Zhang,[a] Jiali Lou,[a] Jiamin Wei,*[a] Yajing Zhou,[a] Haifeng Wang,[b] Liangbiao Wang,[a] Qing Wang[c],

5 Xiaopeng Li *[b] and Xiaokai Song *[a]

6 *[a] Institute of Advanced Functional Materials for Energy, School of Chemistry and*

7 *Chemical Engineering, Jiangsu University of Technology, Changzhou 213001, China.*

8 *[b] Faculty of Science and Engineering, Waseda University, 3-4-1 Okubo, Shinjuku, Tokyo*

9 *169-8555, Japan.*

10 *[c] Jiangsu Key Laboratory of Advanced Catalytic Materials and Technology, Changzhou*

11 *University, Changzhou 213164, China.*

12

1. Experimental Procedures

1.1 Chemicals and materials

2-methylimidazole (98%) and Nafion (5 wt. % in lower aliphatic alcohols and water, contains 15-20% water; Nafion 1100EW) were purchased from Energy Chemical Co., Ltd. and Sigma-Aldrich, respectively. Other reagents and solvents were purchased from Sinopharm Co. Ltd. and used without further purification. Deionized (DI) water with resistivity higher than 18 $M\Omega$ cm^{-1} was used during the experiments.

1.2 Synthesis of MOF nanoparticle and derived superstructure

Truncated rhombic dodecahedral ZIF-8 (TR-Z8). TR-Z8 was prepared by a reported method.[1] In brief, a 25 mL aqueous solution of $Zn(CH_3COO)_2 \cdot 2H_2O$ (1.50 g, 6.8 mmol) was prepared and added to a 25 mL aqueous solution containing 2-methylimidazole (5.60 g, 68 mmol) and cetyltrimethylammonium bromide (CTAB) (5.0 mg, 0.014 mmol), followed by gentle stirring for 1 min. After allowing the mixture to stand undistusbed at room temperature for 2 h, the resulting crystals were collected via centrifugation and washed with water before proceeding to the next step in the synthesis process. The yield of TR-Z8 was determined based on the weight of vacuum-dried sample and used for preparing a colloidal solution with desired concentration in subsequent experiments.

Co^{2+}/ZIF-8 superstructures (Co^{2+}/ZIF-8-x, x represents the dosage of Co^{2+}). Co^{2+}/ZIF-8-10 hybrid superstructure was prepared using an ice-templating assisted self-assembly strategy. Briefly, a stable colloidal solution was obtained by dispersing 300 mg of TR-Z8 nanoparticles and 10 mg of $Co(NO_3)_2 \cdot 6H_2O$ in 30 mL of deionized water, followed by ultrasonication for 30 min. Subsequently, the colloid solution was transferred into a disposable paper cup and slowly immersed into liquid nitrogen for 5 min to achieve complete freezing. After freeze-drying for 24 h using a freeze-dryer, the Co^{2+}/ZIF-8-10 was obtained. Similarly, the Co^{2+}/ZIF-8-0, Co^{2+}/ZIF-8-5, Co^{2+}/ZIF-8-15, and Co^{2+}/ZIF-8-30 were prepared using different amounts of $Co(NO_3)_2 \cdot 6H_2O$ (0 mg, 5 mg, 15 mg and 30 mg, respectively) via this ice-templating assisted self-assembly approach.

1.3 Synthesis of carbon-based catalyst

2D Hollow carbon-based nanoarchitectures (Co/HCS-x). Co/HCS-x was prepared by a high-temperature pyrolysis process under inert atmosphere. Typically, a sample of 300 mg Co^{2+}/ZIF-8-x (Co^{2+}/ZIF-8-0, Co^{2+}/ZIF-8-5, Co^{2+}/ZIF-8-10, Co^{2+}/ZIF-8-15, and Co^{2+}/ZIF-8-30) were calcined in a tube furnace at 900 °C under N_2 atmosphere for 2 h with a temperature raising rate of 3 °C min^{-1}. After natural cooling to room temperature, the catalysts were harvested and designated as Co/HCS-0, Co/HCS-5, Co/HCS-10, Co/HCS-15, and Co/HCS-30, respectively.

1.4 Materials characterization

The morphology and chemical composition of the samples were investigated by scanning electron microscopy (SEM, Hitachi S-3400N) and transmission electron microscopy (TEM, JEOL JEM-2100). The surface chemistry was analyzed by X-ray photoelectron spectroscopy (XPS) performed on a AXISULTRA DLD XPS System with MONO Al source and the binding energies were calibrated using the C 1s peak at 284.8 eV. The phase composition of samples was investigated by X-ray diffraction (XRD, PANalytical X' Pert Powder). The X-ray absorption spectroscopy (XAS) measurements were obtained on the Beam line BL14W1 and BL11B at the Shanghai Synchrotron Radiation Facility (SSRF).

50

1.5 Electrochemical measurements

The electrochemical measurements of ORR performance were tested on a CHI760E electrochemical workstation in a conventional three-electrode system at room temperature. Catalyst ink was prepared by dispersing 5 mg of catalyst in a mixed solution containing 960 μL of ethanol and 40 μL of 5 wt% Nafion solution by ultrasonication to obtain a homogeneous suspension. The electrolytes were composed of 0.1 M KOH. An Ag/AgCl (3M KCl) electrode and a carbon rod were used as reference and counter electrode, respectively. The experiments were conducted at room temperature and all of the potentials were calibrated to a reversible hydrogen electrode (RHE). Generally, a RDE electrode with a diameter of ϕ 3 mm was used as the substrate for the working electrode. An aliquot of 8 μL of the catalyst ink was loaded onto the working electrode and dried under ambient conditions with a mass loading of 0.57 mg cm^{-2}. The electrolyte was purged by a specific gas for at least 30 min before the measurements and the gas flow was maintained during the experiments. Cyclic voltammetry (CV) measurements were conducted at a scan rate of 50 mV s^{-1} and a rotation rate of 1600 rpm. To eliminate the influence of background current, the linear scan voltammetry (LSV) measurements were recorded at a scan rate of 1 mV s^{-1}. The double-layer capacitance (C_{dl}) was measured by a series of CV scanning in a non-Faradaic potential at various scan rates of 5-60 mV s^{-1} in N_2-saturated 0.1 M KOH. The EIS test was carried out from 10^5 Hz to 10^{-2} Hz and recorded at OCP with an amplitude of 10 mV. The tolerance of the electrocatalysts to methanol poisoning was evaluated by injecting 5 mL of 3 M methanol into the electrolyte (150 mL) during the chronoamperometric measurements. For comparison, Pt/C (20 wt% platinum, JM) was conducted on the same electrochemical tests.

To obtain the electron transfer number (n) and hydrogen peroxide yield (% H_2O_2), a rotating ring disk electrode (RRDE) electrode (diameter: ϕ 4 mm) served as working electrode. The catalyst ink (12 μL) was dropped on the RRDE electrode and then dried in the air. The % H_2O_2 and n were calculated as the following equations:

$$\%H_2O_2 \ = \ 200 \times \frac{I_R/N}{I_D + I_R/N} \tag{1}$$

$$n \ = \ \frac{4}{1 + \frac{I_R}{I_D} \times N} \tag{2}$$

Where I_D and I_R are the disk and ring currents, respectively, and N is the collection efficiency (37%) of the ring electrode.

The rotating speed of RDE was controlled from 400 to 2025 rpm. The Koutecký-Levich equation is:

$$\frac{1}{j} = \frac{1}{j_L} + \frac{1}{j_K} = \frac{1}{B\omega^{1/2}} + \frac{1}{j_K} \tag{3}$$

$$B = 0.62nFC_0(D_0)^{2/3} \nu^{-1/6} \tag{4}$$

$$j_K = nFkC_0 \tag{5}$$

Where j is the measured current density, j_K and j_L are the kinetic- and diffusion-limiting current densities, ω is the angular velocity of the disk ($\omega = 2\pi N$, N is the linear rotation speed), n represents the overall number of electrons transferred in oxygen reduction, F is the Faraday constant (F = 96485 C mol^{-1}), C_0 is the bulk concentration of O_2 (1.2×10^{-6} mol cm^{-3}), D_0 is the diffusion coefficient of O_2 in 0.1 M KOH electrolyte (1.9×10^{-5} cm^2 s^{-1}), ν is the kinematic viscosity of the electrolyte (0.01 cm^2 s^{-1}), and k is the electron transfer rate constant.

1.6 Zinc air batteries (ZABs) measurement

1.6.1 Liquid ZABs

Liquid ZABs were assembled in a typical two electrode configuration, in which a metallic zinc foil of purity

88 ~99.9% and an air electrode were used as anode and cathode, respectively. The air electrode used a carbon paper-
89 based gas diffusion layer (TORAY-YLS 30T). The catalyst ink was drop casted onto the gas diffusion layer and dried
90 by a hot air gun (temperature set at 80 °C). The catalyst loading was controlled to 1.0 mg cm^{-2}. The electrolyte was
91 aqueous 6 M KOH with 0.2 M zinc acetate, which was constantly purged with pure oxygen at a rate of 40 mL min^{-1}.
92 Prior to performance tests, the electrolyte was also purged with oxygen for 30 min in order to saturate electrolyte
93 with oxygen. The open circuit voltage, discharging and charging polarization curves were recorded using the
94 CHI760E electrochemical workstation. Rate performance of the assembled ZABs were evaluated by recording
95 voltage profiles during galvanostatic discharge at various current densities from 5 to 50 mA cm^{-2}. The constant
96 current discharge-charge cycle curves and specific capacity of the batteries were carried out at room temperature
97 using a battery test system (Land 3001A). The ZABs were discharged for 150 second and charged for 150 second at
98 a current density of 10 mA cm^{-2} in each galvanostatic cycle. The specific capacity and energy density were calculated
99 according to the following equations:

$$\text{Specific capacity (mAh·g}^{-1}) = I \times t/w_{Zn} \tag{6}$$

101 where I is the applied current (A), t is the serving time (s), V is the average discharge voltage (V), and w_{Zn} is
102 the weight of zinc consumed (g).

1.6.2 Flexible ZABs

104 Flexible solid-state ZAB is consisted of air electrode, polyacrylic acid (PAA) film and zinc foil, which were
105 served as air electrode, solid electrolyte and anode, respectively. The air electrode consists of a piece of nickel foam
106 (NF) on the air-facing side as the current collector, a gas diffusion layer (GDL) in the middle, and a carbon cloth
107 layer coated with catalyst (catalyst loading of 1.0 mg cm^{-2}) on the electrolyte-facing side. To prepare PAA gel
108 electrolyte: 1 g of N, N-methylene diacrylamide as a cross-linker and 5 g of acrylic acid were quickly poured into 20
109 mL of DI water containing 18 g of KOH under continuous stirring, followed by dissolving 1.5 g of zinc acetate.
110 After stirring for 2 h, $K_2S_2O_8$ aqueous solution (0.12 g dissolved in 20 mL of DI water) as the initiator was added to
111 the aforementioned solution in the square mold and then shaken vigorously to form the PAA gel. The polarization
112 curves were recorded via linear sweep voltammetry (LSV) at room temperature on a CHI 760E electrochemical
113 working station. Both the current density and power density were normalized to the effective surface area of the air
114 electrode. The ZABs were discharged for 150 second and charged for 150 second at a current density of 1 mA cm^{-2}
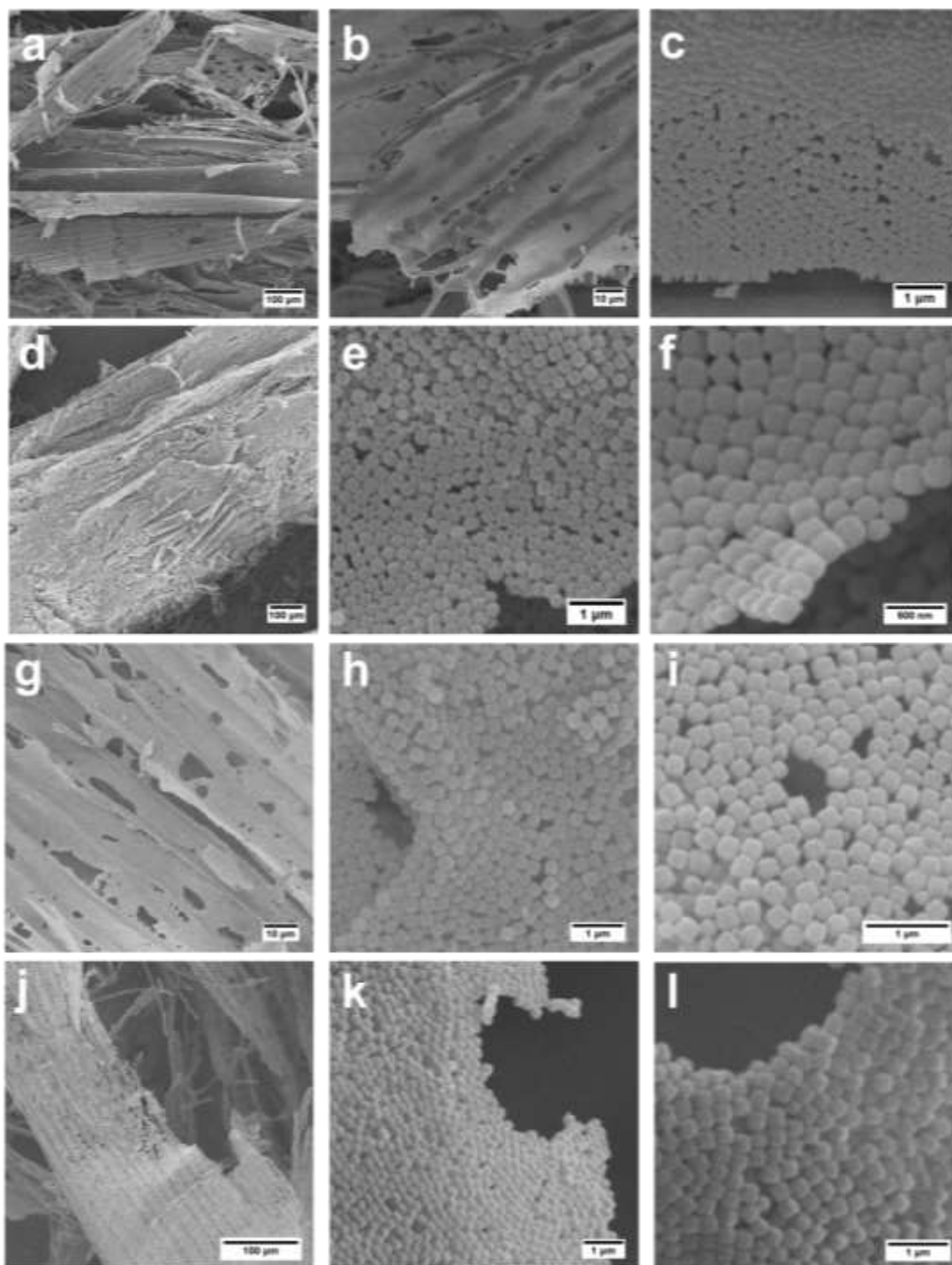115 in each galvanostatic cycle.

116

117 **2. Results and Discussion**

118
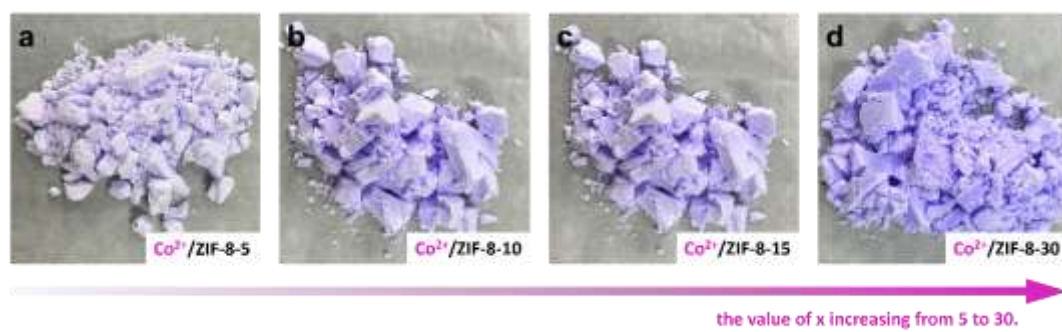
Fig. S1 Digital photographs of ice-templating co-assembled $Co^{2+}/ZIF-8-x$. (a) $Co^{2+}/ZIF-8-5$, (b) $Co^{2+}/ZIF-8-10$, (c) $Co^{2+}/ZIF-8-15$, and (d) $Co^{2+}/ZIF-8-30$.

122

Fig. S2 SEM images of Co^{2+}/ZIF-8-x. (a-c) Co^{2+}/ZIF-8-5, (d-f) Co^{2+}/ZIF-8-10, (g-i) Co^{2+}/ZIF-8-15, and (j-l) Co^{2+}/ZIF-8-30.

126
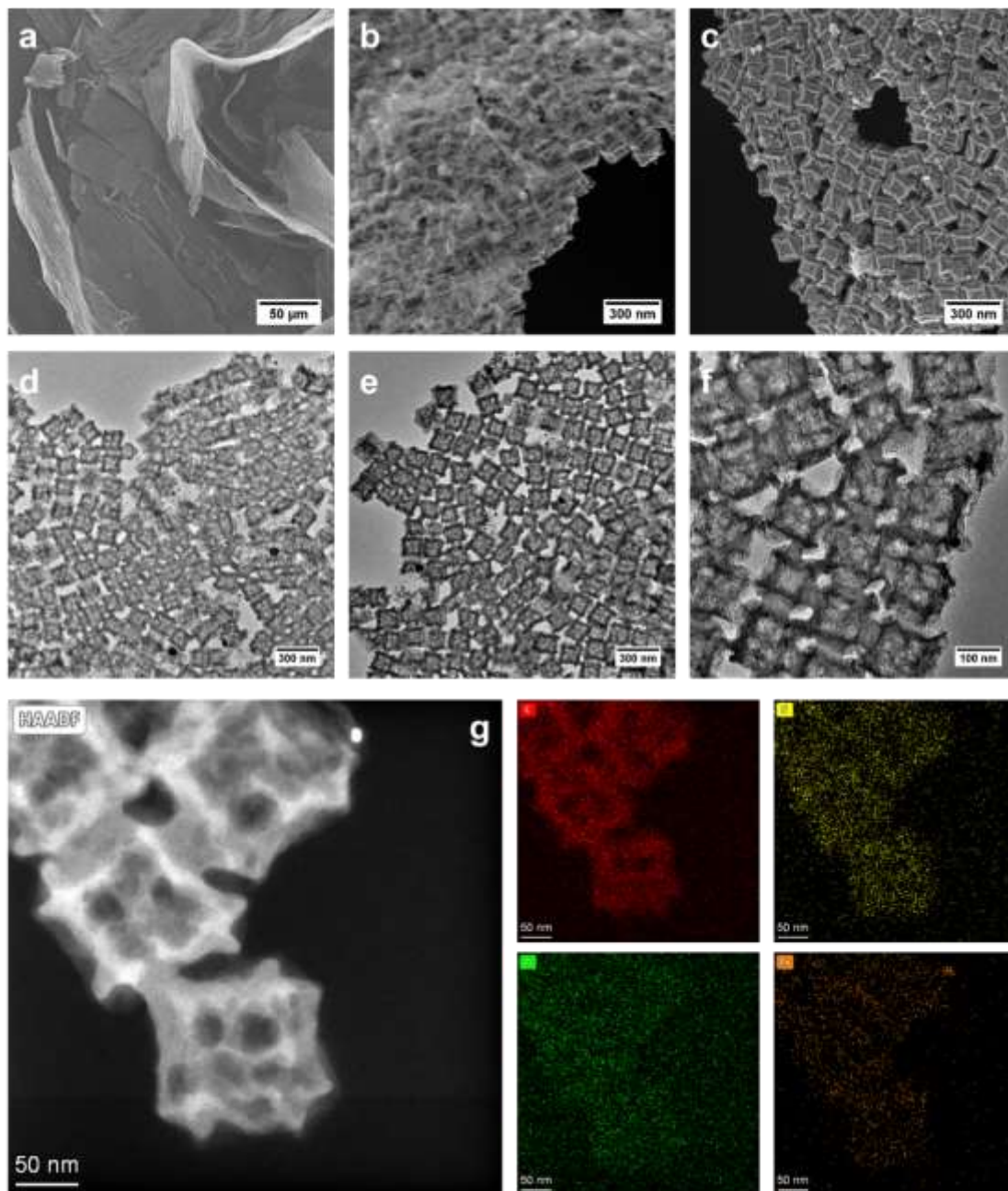
Fig. S3 (a-c) SEM images, (d-f) TEM images, and (g) scanning TEM (STEM) images and elemental mapping images of 2D Co/HCS-10.

130
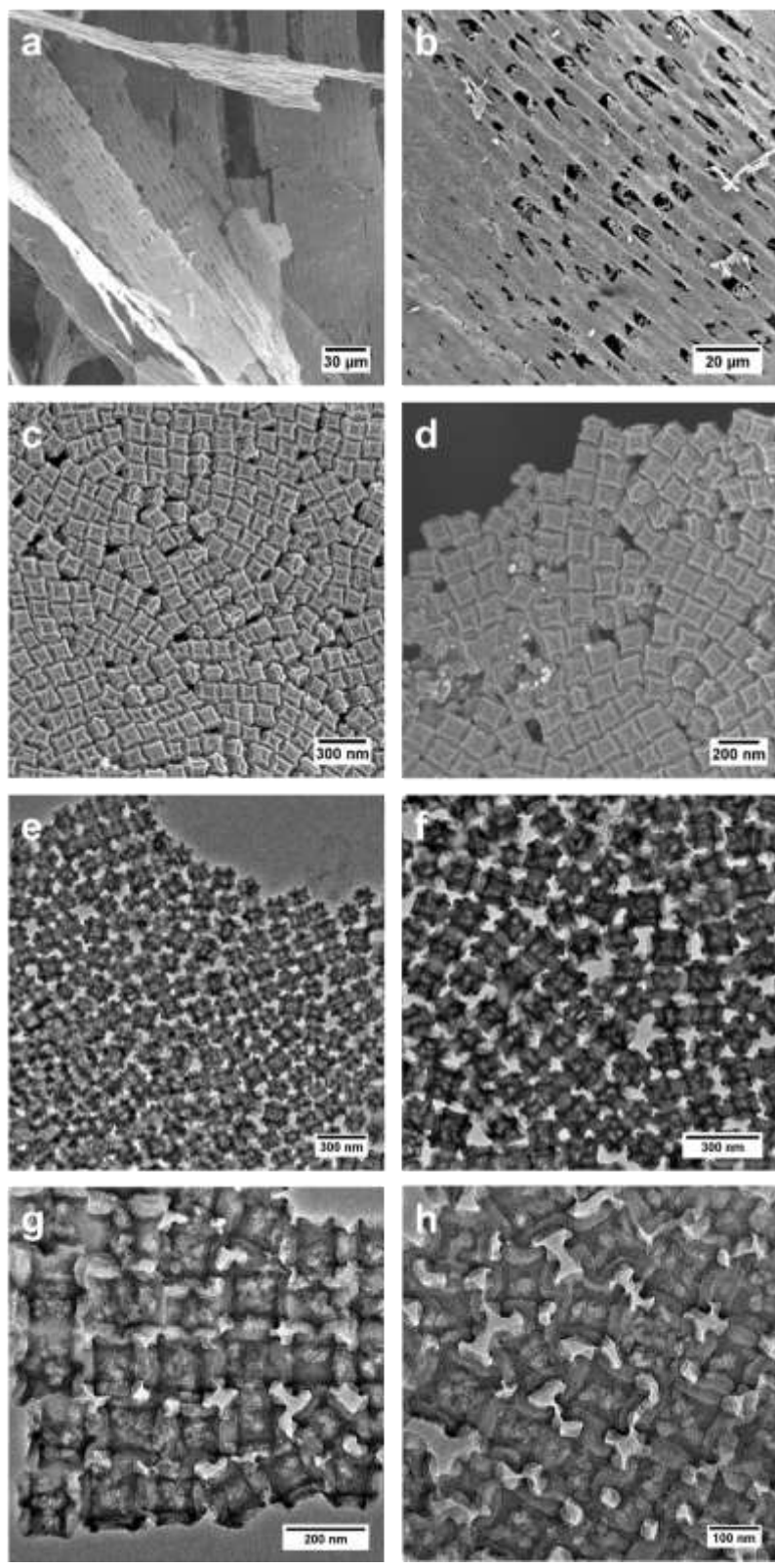
Fig. S4 (a-d) SEM and (e-h) TEM images of 2D Co/HCS-5.
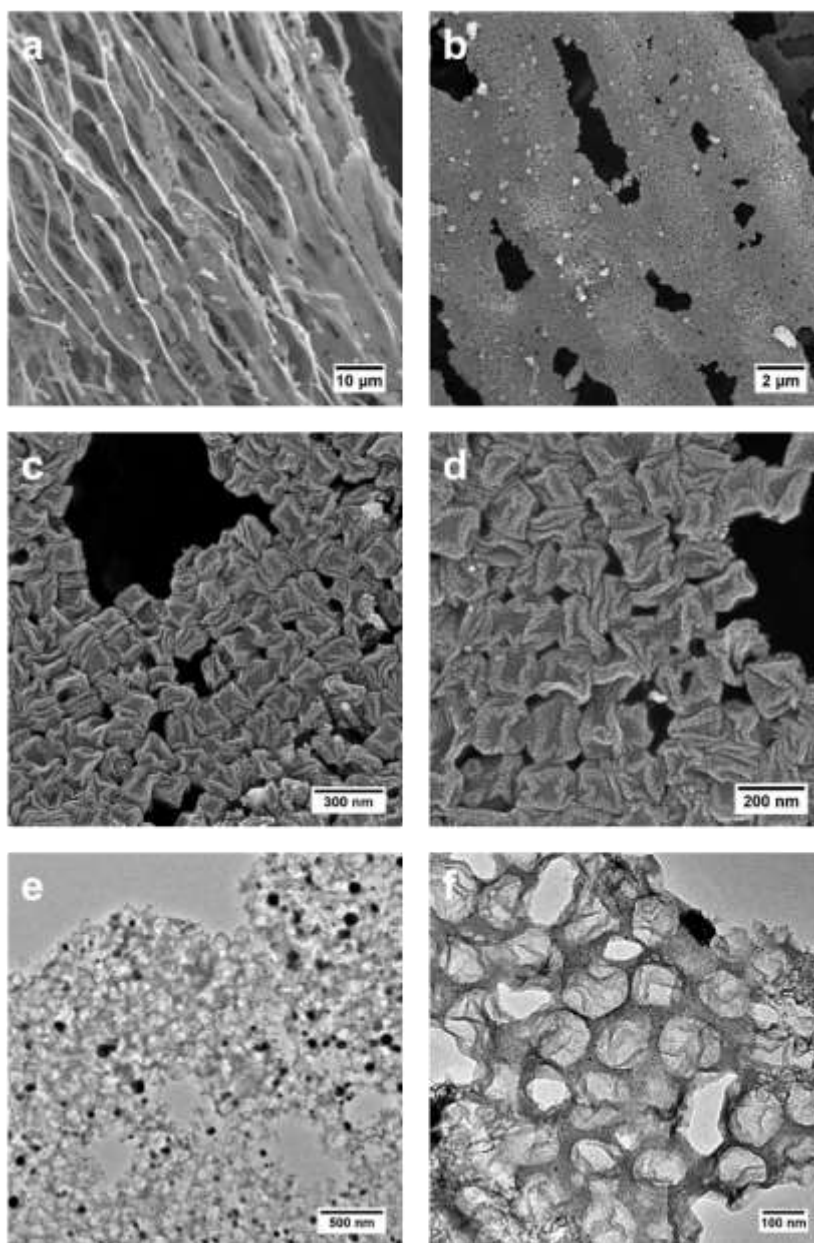
133

134 **Fig. S5** (a-d) SEM and (e,f) TEM images of 2D Co/HCS-15.

135
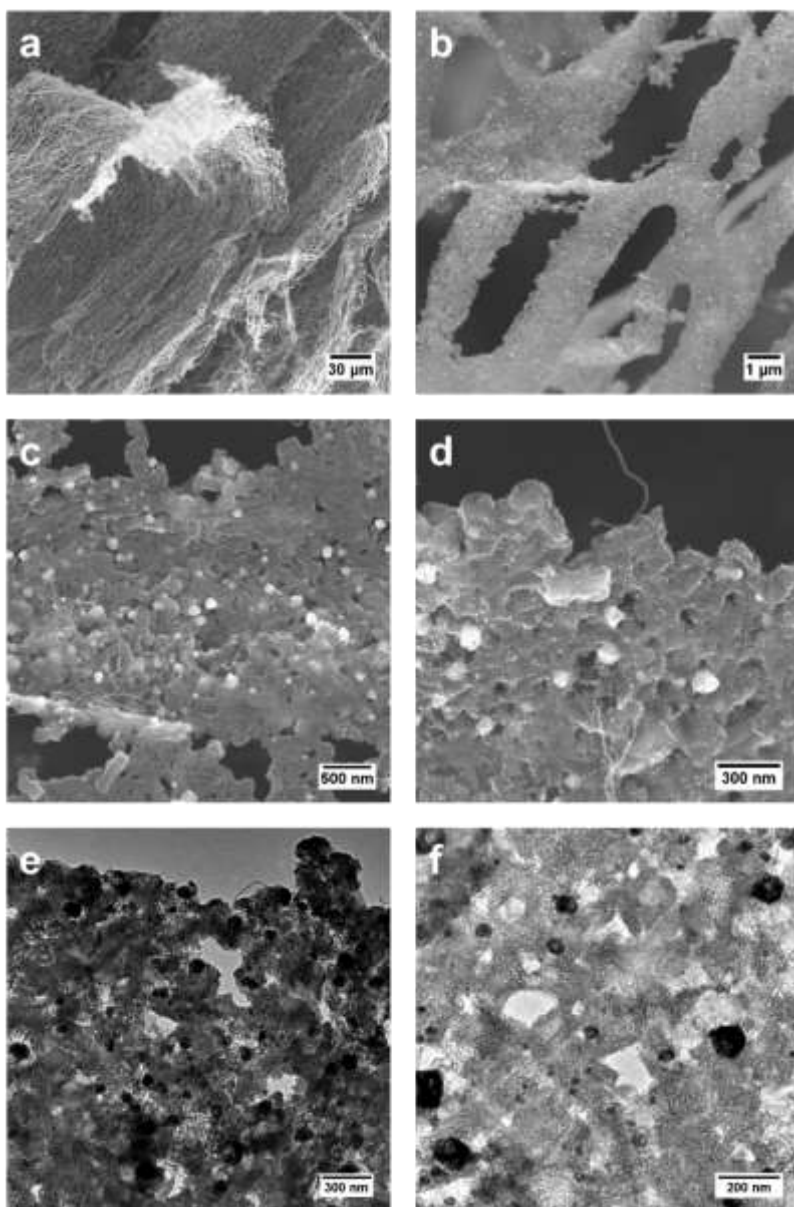
136

137   **Fig. S6** (a-d) SEM and (e,f) TEM images of 2D Co/HCS-30.

138

139
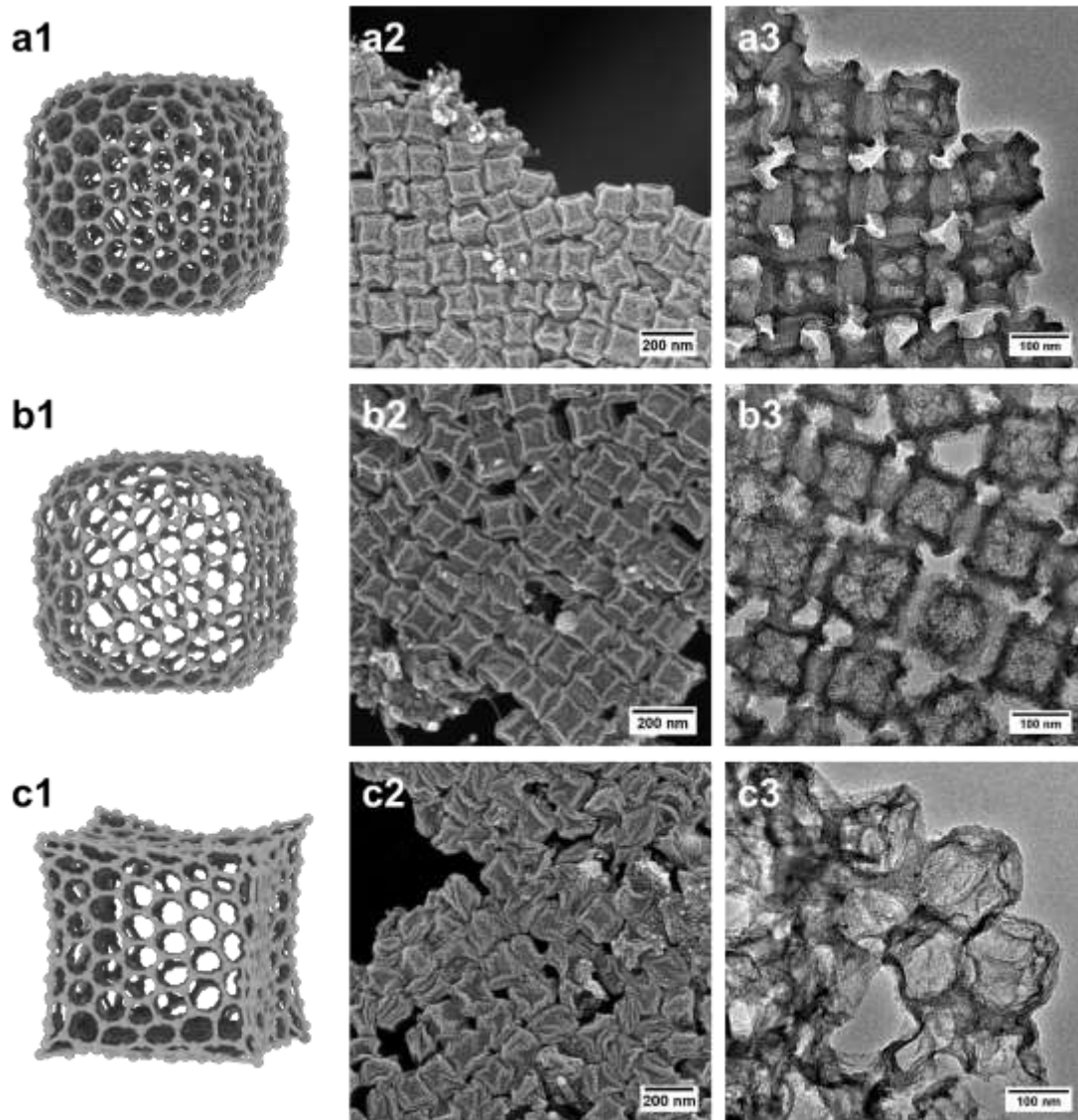
Fig. S7 Structural comparison of Co/HCS-5, Co/HCS-10 and Co/HCS-15. Schematic illustration, SEM and TEM
images of (a) Co/HCS-5, (b) Co/HCS-10, and (c) Co/HCS-15.

143
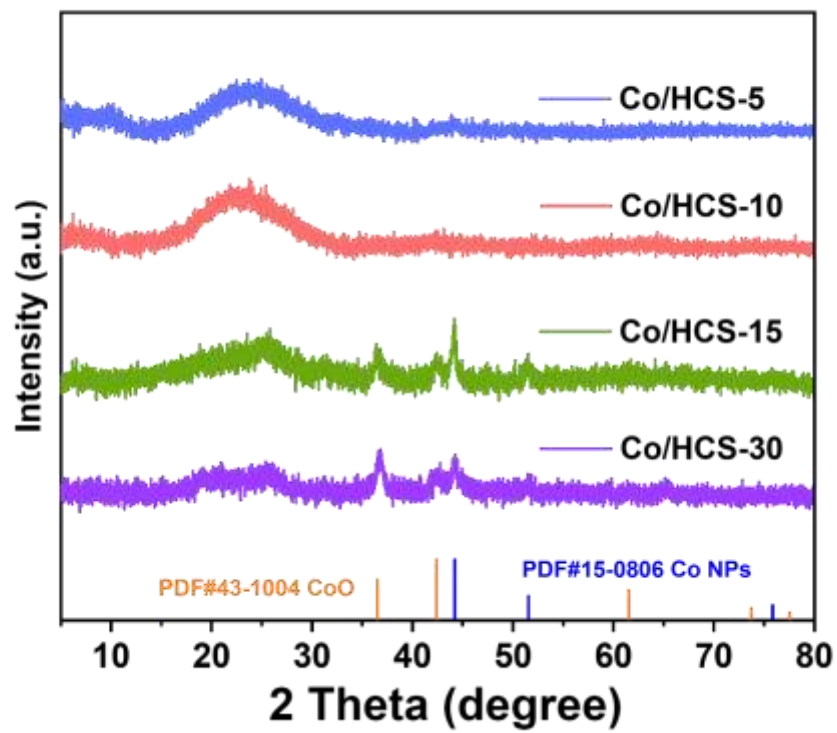
Fig. S8 Powder X-ray diffraction (PXRD) patterns of Co/HCS-5, Co/HCS-10, Co/HCS-15, and Co/HCS-30.

145
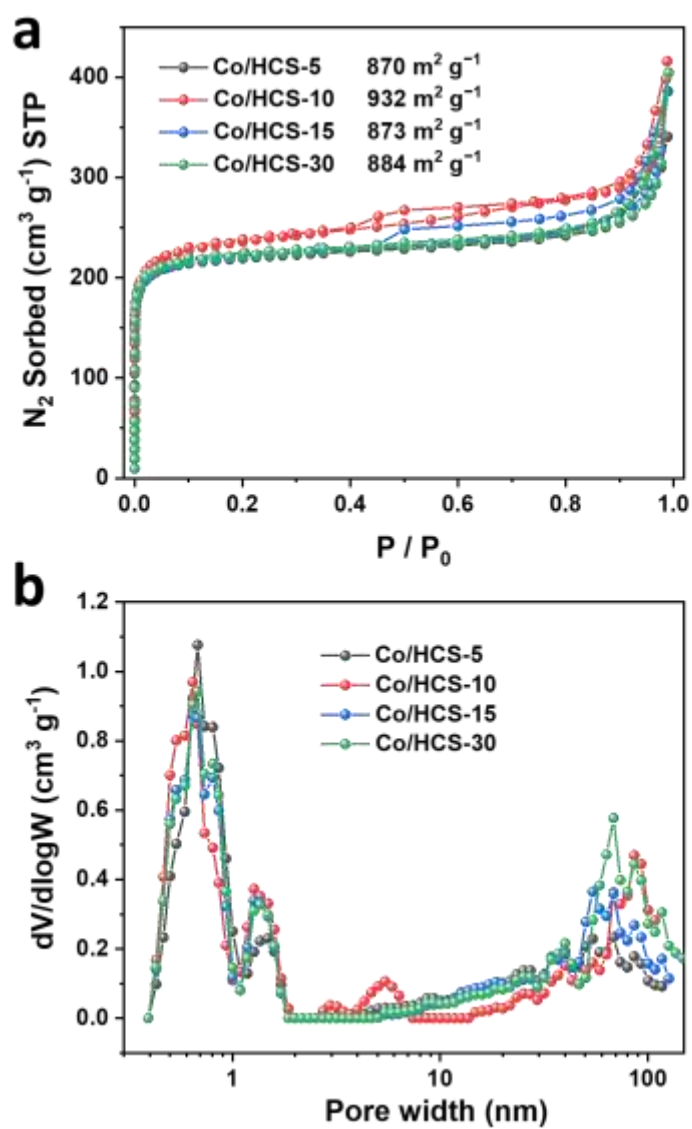
146

147 **Fig. S9 (**a) N_2 adsorption/desorption isotherms and (b) NLDFT pore size distribution plots of Co/HCS-5, Co/HCS-
148 10, Co/HCS-15, and Co/HCS-30.
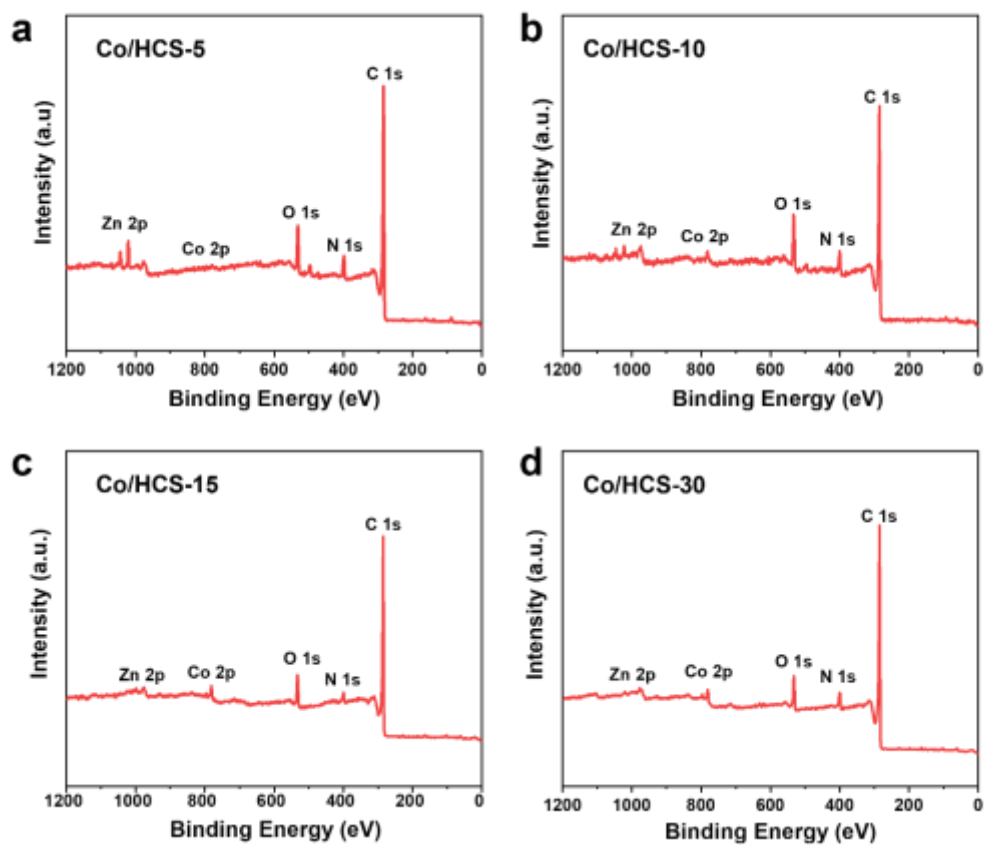
149

150   **Fig. S10** XPS survey spectra of Co/HCS-5, Co/HCS-10, Co/HCS-15, and Co/HCS-30.

151

152
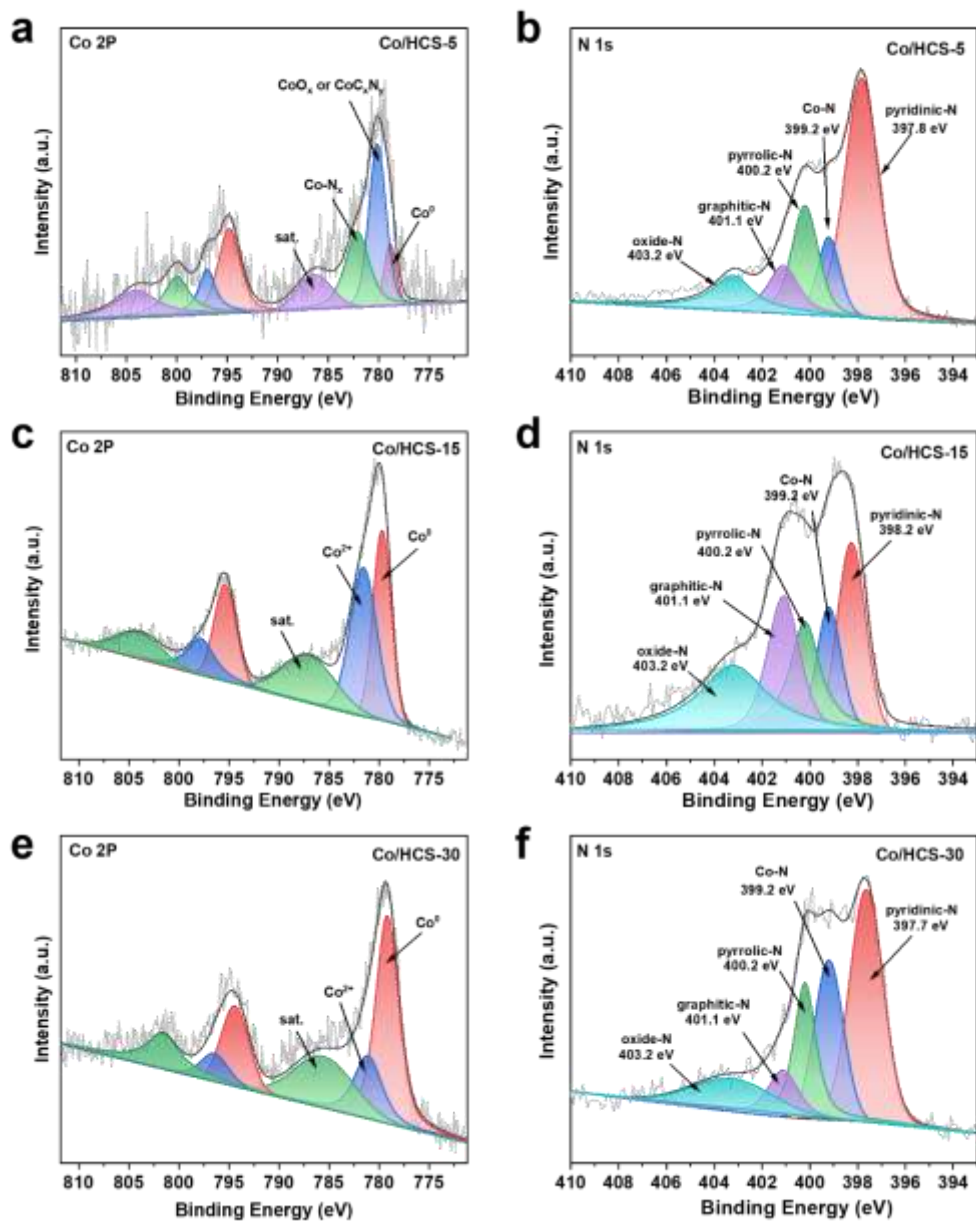
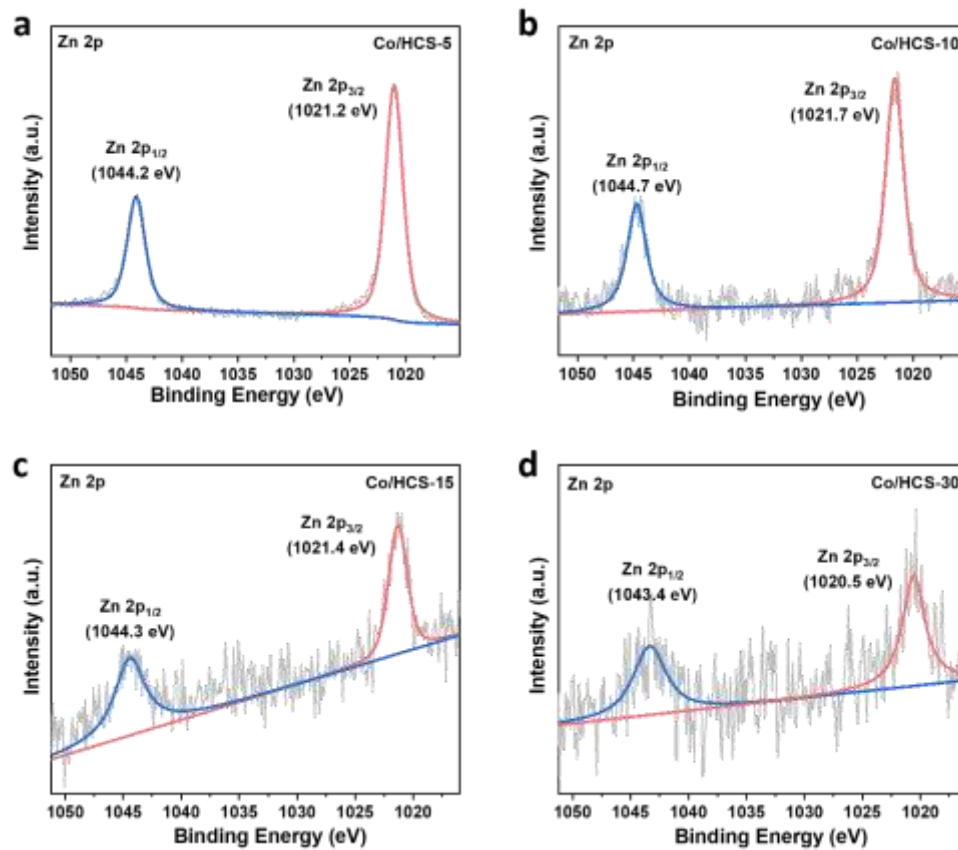**Fig. S11** High-resolution deconvoluted Co 2p, and N 1s XPS spectra of (a,b) Co/HCS-5, (c,d) Co/HCS-15, and (e,f)
Co/HCS-30.
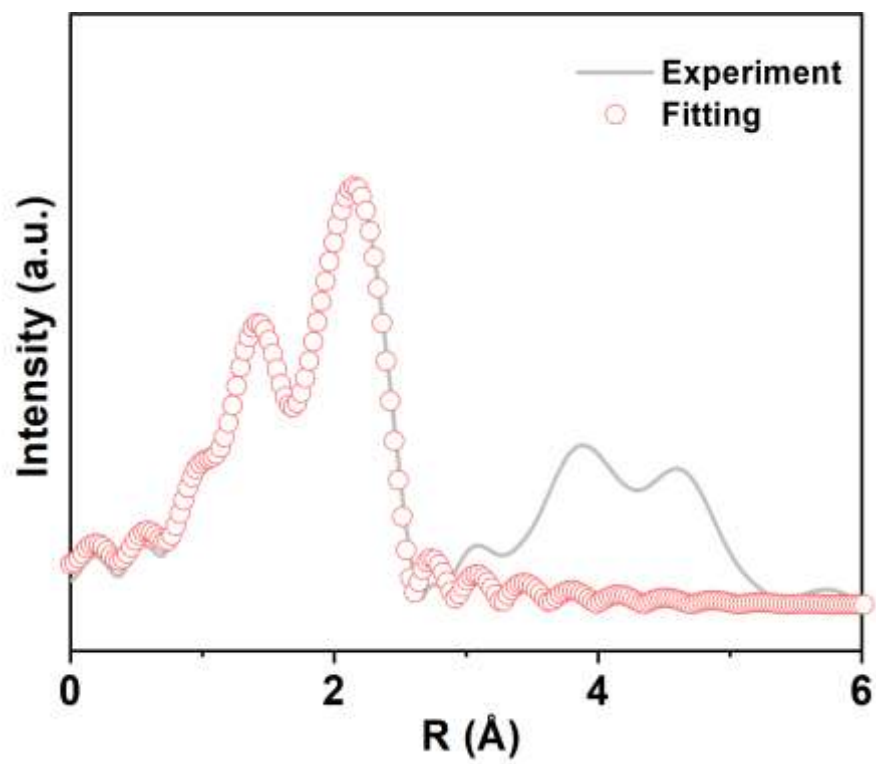
156

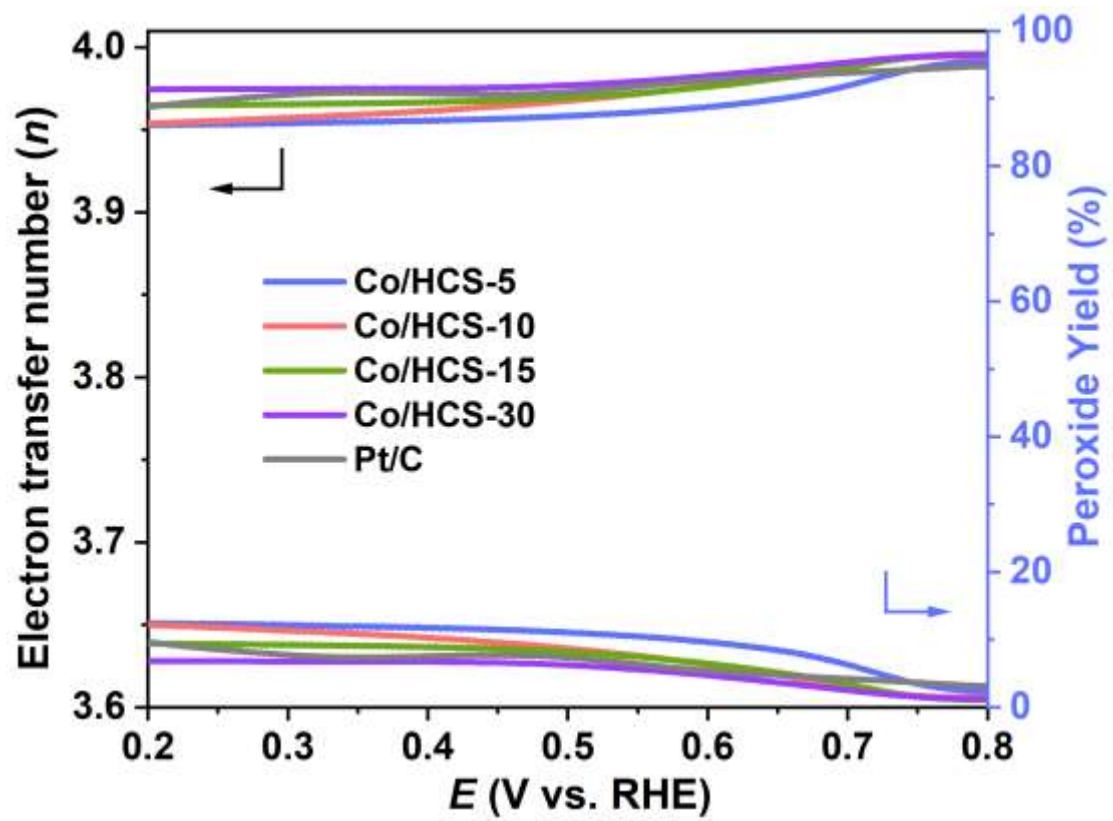157   **Fig. S12** The EXAFS fitting curves of Co/HCS-10.

158

Fig. S13 High-resolution deconvoluted Zn 2p XPS spectra of (a) Co/HCS-5, (b) Co/HCS-10, (c) Co/HCS-15, and (d) Co/HCS-30.
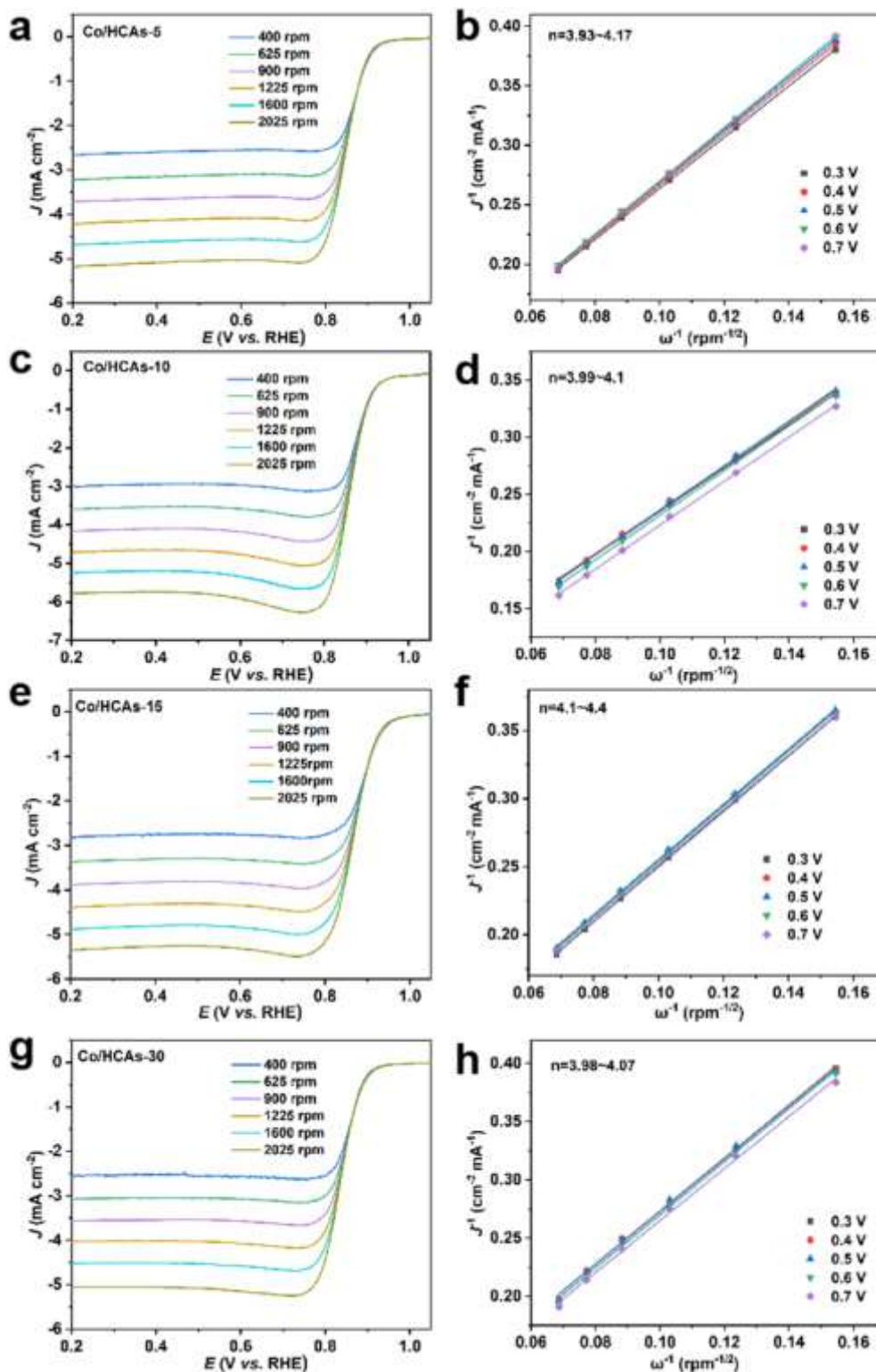
164
165 **Fig. S14** The electron transfer number and H₂O₂ yield plots.
166
167

168

Fig. S15 LSV curves at a scan rate of 2 mV s⁻¹ in 0.1 M KOH with rotating speed from 400 to 2025 rpm. (a) ORR polarization curves of Co/HCS-5, and (b) corresponding K–L plots. (c) ORR polarization curves of Co/HCS-10, and (d) corresponding K–L plots. (e) ORR polarization curves of Co/HCS-15, and (f) corresponding K–L plots. (g) ORR polarization curves of Co/HCS-30, and (h) corresponding K–L plots.
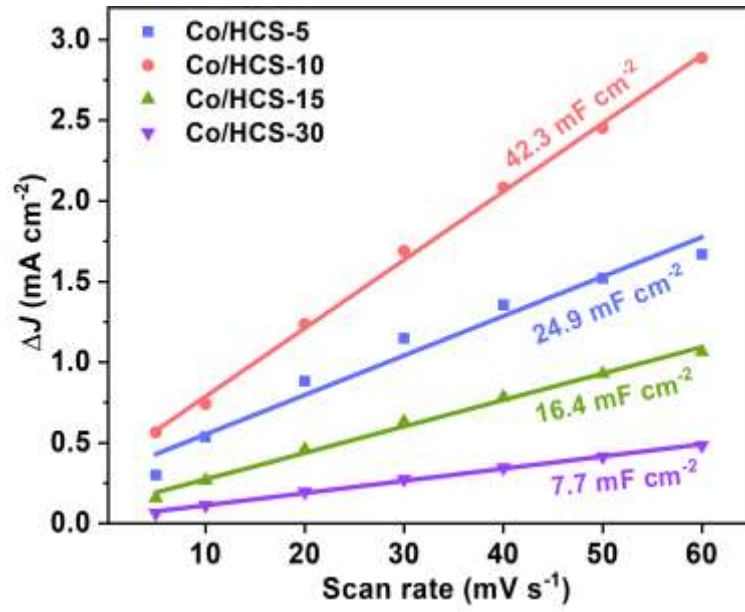
174
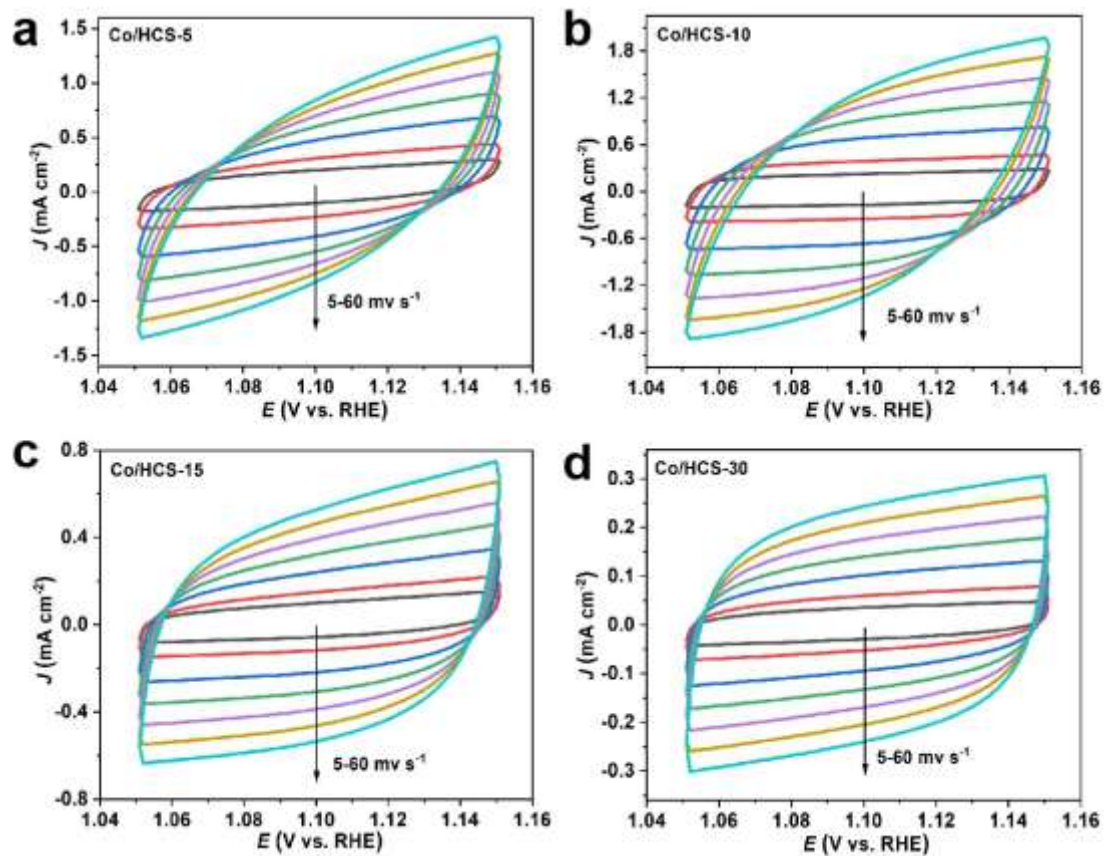
Fig. S16 The cyclic voltammograms curves in the non-faradaic region at different scan rates: (a) Co/HCS-5, (b) Co/HCS-10, (c) Co/HCS-15, (d) Co/HCS-30.
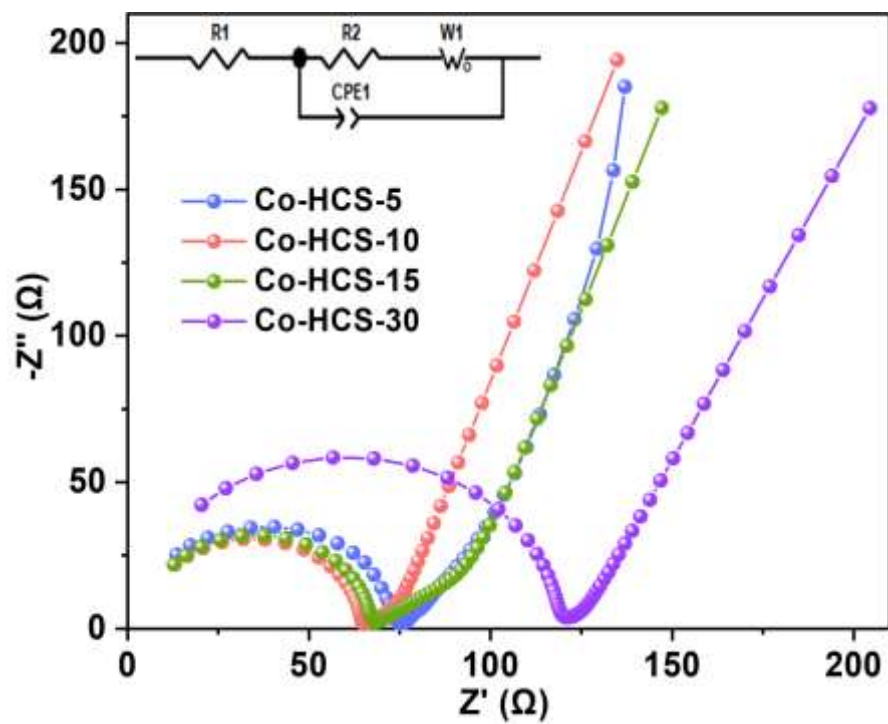
178

179   **Fig. S17** Electrochemical double-layer capacitances (C_{dl}) of Co/HCS-5, Co/HCS-10, Co/HCS-15, and Co/HCS-30.
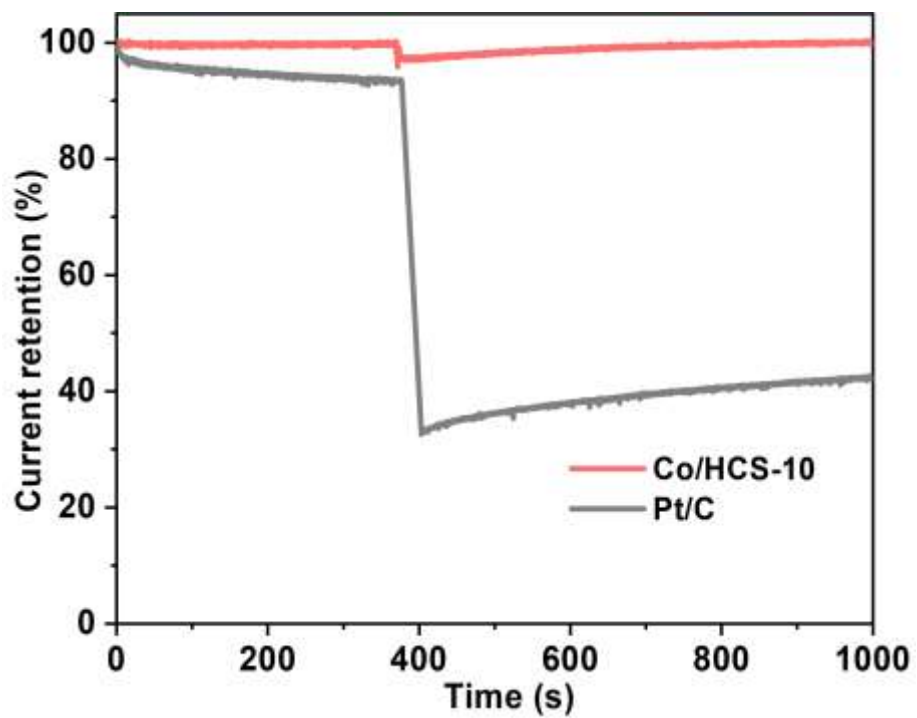
180

181

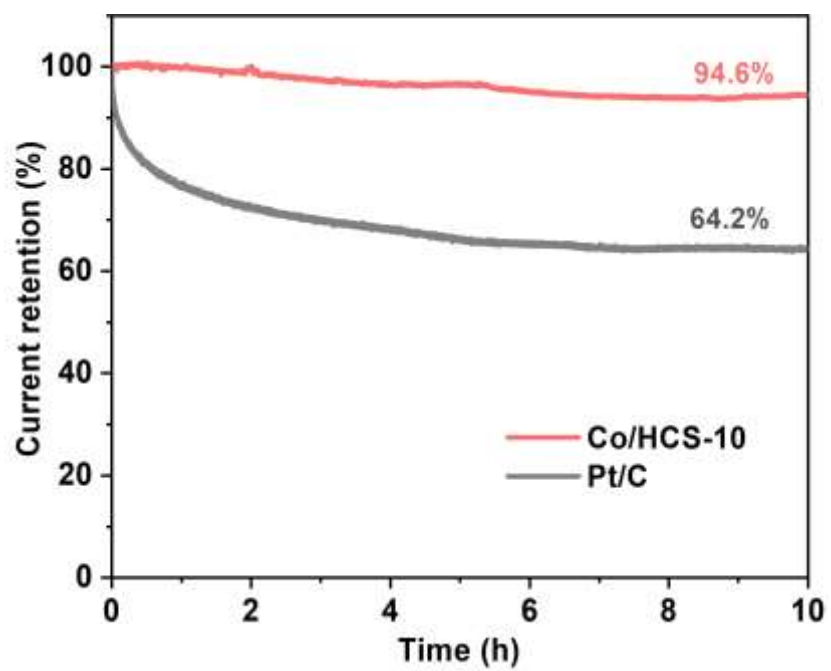Fig. S18 EIS spectra at open circuit potential for Co/HCS-5, Co/HCS-10, Co/HCS-15, Co/HCS-30.

182

183

184

Fig. S19 Chronoamperometric responses of Co/HCS-10 and Pt/C before and after the addition of methanol.
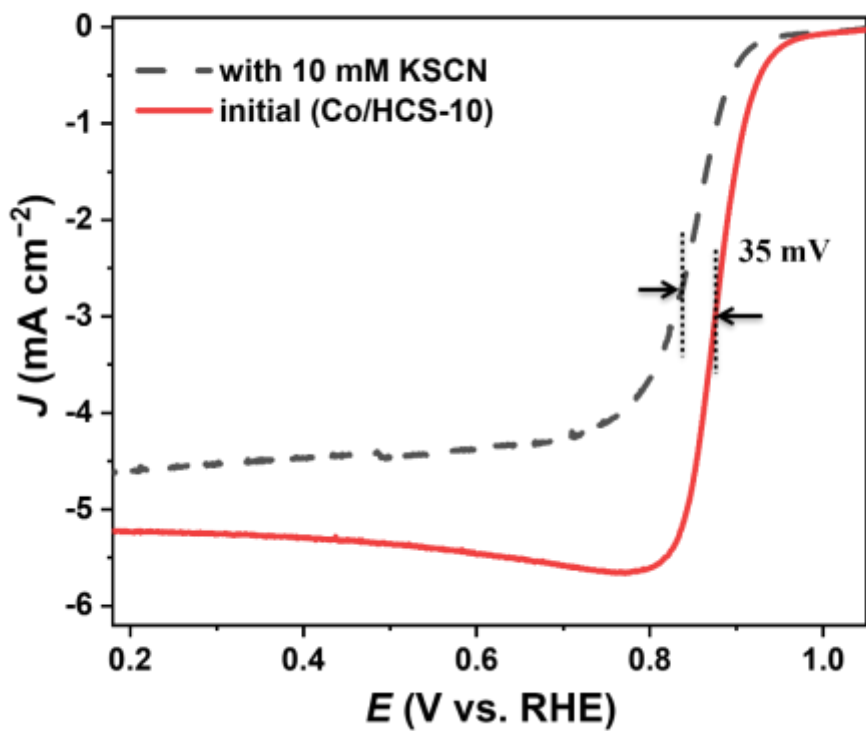
186

187

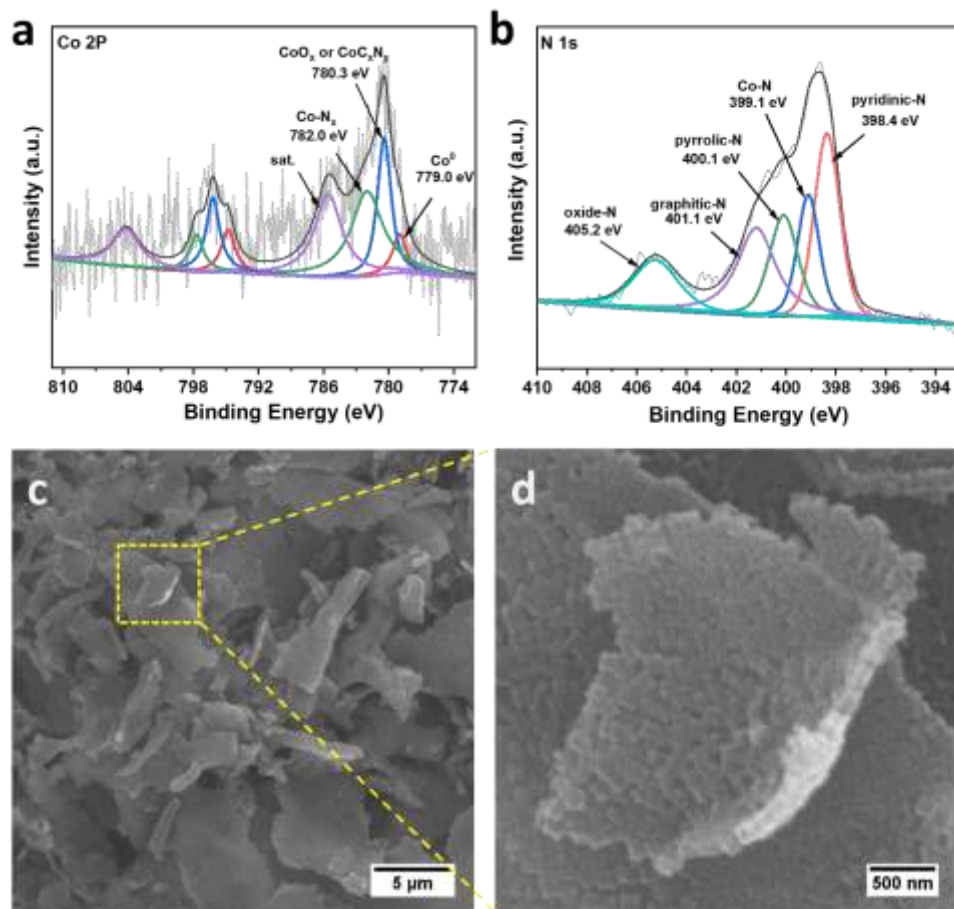**Fig. S20** Current retention from chronoamperometric curves of Co/HCS-10 and Pt/C.

189

190

191   **Fig. S21** ORR polarization curves of Co/HCS-10 before and after KSCN injection.

192

Fig. S22 (a,b) High-resolution deconvoluted Co 2p and N 1s XPS spectra, and (c,d) SEM images of Co/HCS-10 after the stability test.

The 2D Co/HCS-10 catalyst is quite robust, because these superstructured carbon particles are closely connected together. When we applied strong ultrasonication to prepare catalyst ink, the unique 2D superstructure remains structurally stable after the stability testing. Additionally, XPS analysis of used Co/HCS-10 indicates no obvious chemical state changes after stability test.
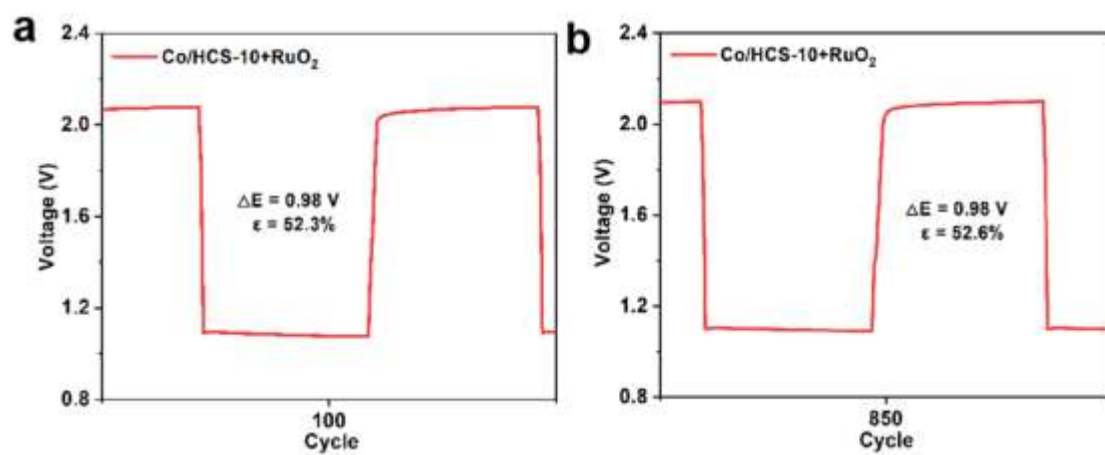
201
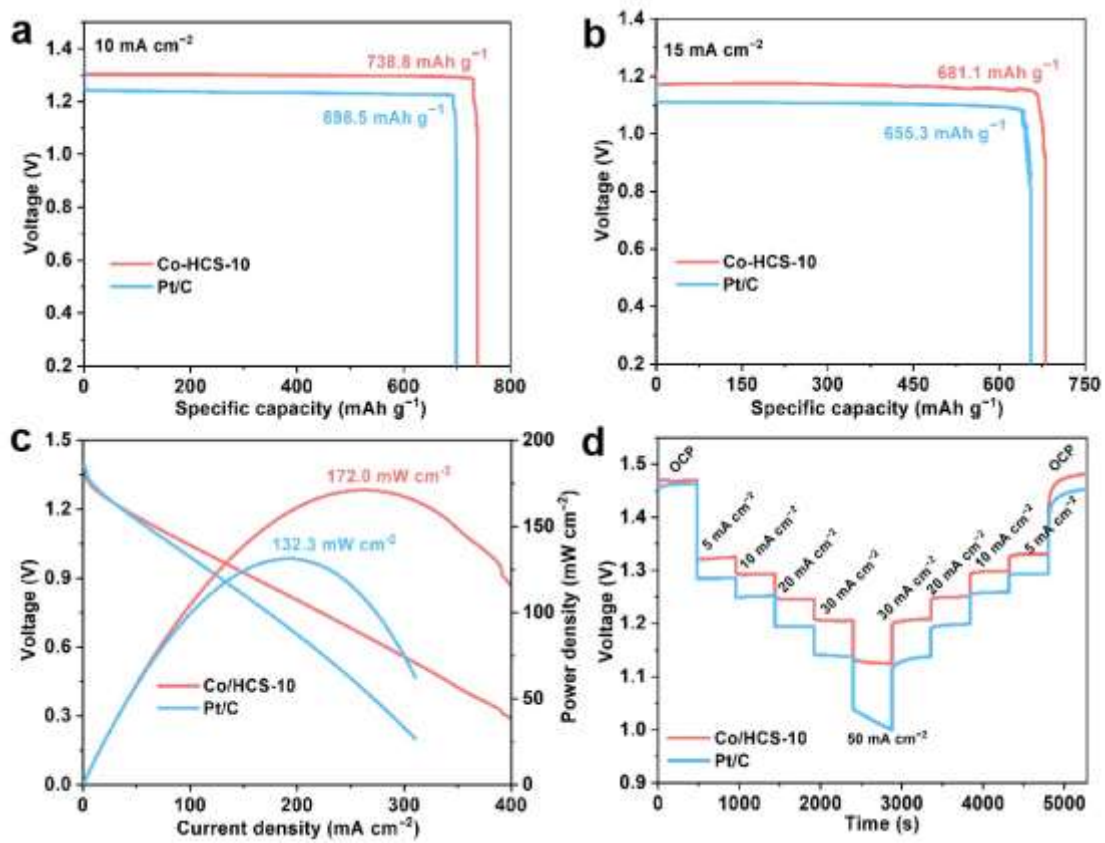
Fig. S23 The liquid ZABs performance comparison between Co/HCS-10 and Pt/C catalysts. Galvanostatic discharge curves at (a) 10 mA cm^{-2}, and (b) 15 mA cm^{-2}. (c) Discharging polarization and power density curves. (d) Galvanostatic rate performance at various current densities.

202

203

204

205
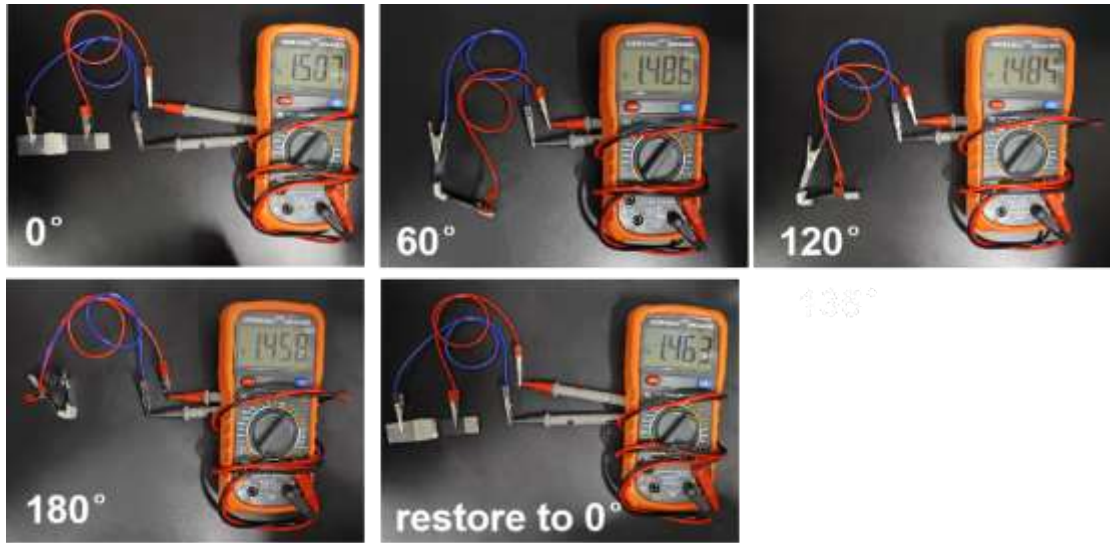
206

207

Fig. S24 (a-b) The 100th and 850th discharge/charge cycle curves of the the liquid ZABs equipped with Co/HCS-10+RuO$_2$ cathode (The charge and discharge plateau voltages used here are their average values).
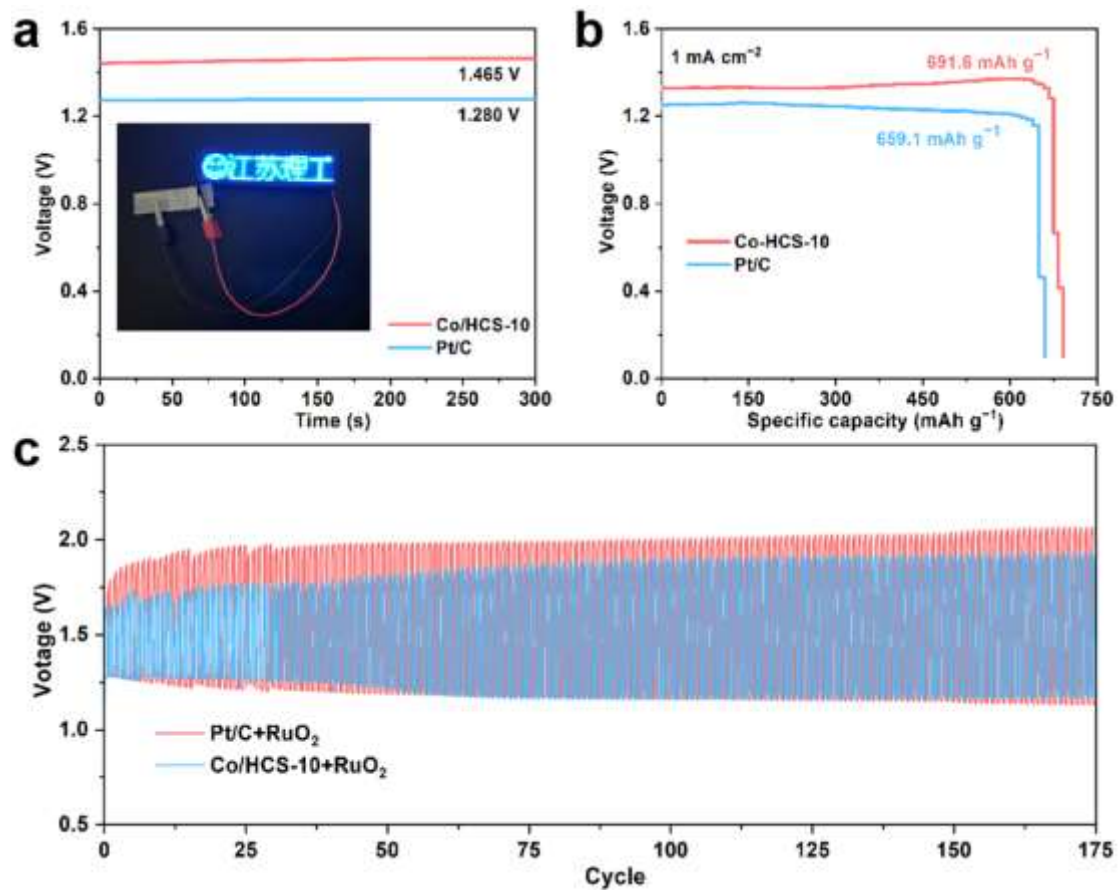
211

212 **Fig. S25** The open circuit voltage of the flexible ZABs equipped with Co/HCS-10 cathode under different bending
213 angles.
214

215

Fig. S26 The flexible ZABs performance comparison between Co/HCS-10 and Pt/C catalysts. (a) The open circuit voltage plots. (d) The specific capacities at 1 mA cm^{-2}. (c) The galvanostatic discharge/charge cycling stability.

220 **Table S1**. Elemental composition of Co/HCS-5, Co/HCS-10, Co/HCS-15, and Co/HCS-30 determined by XPS.

Sample	C(at%)	N(at%)	O(at%)	Co(at%)	Zn(at%)
Co/HCS-5	81.21	7.94	9.48	0.36	1.01
Co/HCS-10	80.64	7.58	10.22	0.97	0.59
Co/HCS-15	86.45	4.28	8.24	0.85	0.18
Co/HCS-30	87.45	5.4	6.09	0.83	0.23

221

222 **Table S2**. Structural parameters extracted from the Co K-edge EXAFS fitting of Co/HCS-10.

sample	shell	N	R (Å)	$\sigma^2(10^{-3}Å^2)$	ΔE_0 (eV)	R factor
Co/HCS-10	Co-N	3.2	1.95	9.4	-4.9	0.004

223 N, coordination numbers; R, the internal atomic distance; σ^2, the Debye-Waller factor; ΔE_0, inner

224 potential correction to account for the difference in the inner potential between the sample and the

225 reference compound; R factor, indicates the goodness of the of the fitting.

226

227 **Table S3**. Comparison of liquid ZABs performance with other reported transition metal based electrocatalysts.

Smaple	Open Voltage (V)	Peak power density (mW cm^{-2})	Ref
Co/HCS-10	1.486	172.0	this work
RuCo/NPC (5:5)‖RuCo/NPC (7:3)	1.45	79.4	*Chem. Commun.* **2021**, 57,1498-1501
CoCu/N-CNS	1.424	104.3	*Small* **2023**, 19, 2207413
Co-CoN$_4$@NCNs	1.47	131.6	*Adv. Funct. Mater.* **2022**, 32, 2207331
CoP$_3$/CeO$_2$/C	1.343	150.0	*Appl. Catal. B: Environ.* **2023,** 321, 122029
Pt@CoS$_2$-NrGO	1.41	114	*Appl. Catal. B: Environ.* **2021**, 297, 120405
Co SA/NCFs	1.53	154.5	*Nano Lett.* **2022**, 22, 2497–2505
FeP/Fe$_2$O$_3$@ NPCA	1.428	130.0	*Adv. Mater.* **2020**, 2002292
Fe-P/Cu$_3$P-NPC	1.39	158.5	*Small* **2023**, 2301985

228

229

230